Ultrafast X-ray pulse characterization at free-electron lasers

I. Grguraš[1†], A. R. Maier[2,3†], C. Behrens[4†], T. Mazza[5], T. J. Kelly[6], P. Radcliffe[5], S. Düsterer[4], A. K. Kazansky[7,8,9], N. M. Kabachnik[5,9,10], Th. Tschentscher[5], J. T. Costello[6], M. Meyer[5], M. C. Hoffmann[1,11], H. Schlarb[4] and A. L. Cavalieri[1*]

The ability to fully characterize ultrashort, ultra-intense X-ray pulses at free-electron lasers (FELs) will be crucial in experiments ranging from single-molecule imaging to extreme-timescale X-ray science. This issue is especially important at current-generation FELs, which are primarily based on self-amplified spontaneous emission and radiate with parameters that fluctuate strongly from pulse to pulse. Using single-cycle terahertz pulses from an optical laser, we have extended the streaking techniques of attosecond metrology to measure the temporal profile of individual FEL pulses with 5 fs full-width at half-maximum accuracy, as well as their arrival on a time base synchronized to the external laser to within 6 fs r.m.s. Optical laser-driven terahertz streaking can be utilized at any X-ray photon energy and is non-invasive, allowing it to be incorporated into any pump–probe experiment, eventually characterizing pulses before and after interaction with most sample environments.

Theoretical studies and user operations at the extreme ultraviolet (XUV) and soft X-ray free-electron laser in Hamburg (FLASH)[1], at the hard X-ray Linac Coherent Light Source at the SLAC National Accelerator Laboratory[2] and at the SPring-8 Angstrom Compact Free Electron Laser at RIKEN Harima Institute[3,4] indicate that free-electron lasers (FELs) can deliver pulses with durations in the range of tens of femtoseconds to less than a femtosecond with $\sim 10^{11}$–10^{13} photons per pulse[5,6]. The unique combination of unprecedented brightness and ultrashort pulse duration ensures new possibilities for high-resolution time-resolved X-ray studies[7,8], for experiments involving high-intensity X-ray–matter interaction[9–11], and will allow for a new class of biomolecular imaging experiments[12–14].

However, at present, X-ray FELs rely primarily on the stochastic process of self-amplified spontaneous emission (SASE) and emit pulses without a well-defined temporal profile. SASE FEL pulses are composed of independent, temporally coherent emission spikes. The duration of these spikes can range from hundreds of attoseconds to several femtoseconds depending on the coherence length of the FEL process[15]. The full length of the intensity envelope formed by the stochastically distributed emission spikes is expected to be 100 fs or less, and it may fluctuate dramatically from shot to shot as a result of phase space density variations across the driving electron bunch. Therefore, in experiments where dynamic processes are expected to occur during FEL exposure, such as in biological imaging where the onset of radiation damage is expected to occur within the first few femtoseconds, the FEL pulse profile must be measured with femtosecond accuracy on a single-shot basis.

In two-colour, time-resolved experiments using an optical laser and a FEL, significant temporal jitter and drift exist between the two distinct sources of pump and probe. Without additional information, the exact delay between excitation and observation is unknown and the time resolution is reduced to the level of the timing jitter. The largest contribution to timing jitter is caused by insufficient synchronization between the optical laser pulse and the FEL-driving electron bunch. When timing is required with a resolution equivalent to or better than the FEL pulse duration, shot-to-shot fluctuation in the regions or portion of the electron bunch that generate SASE-amplified radiation become a significant source of additional jitter.

Insufficient synchronization can be mitigated by simple time-of-arrival measurements of the electron bunch with respect to the pump laser pulse[16–18]. However, these measurements cannot be used to address fluctuations in SASE amplification over the length of the electron bunch and they introduce an internal source of unaccounted timing jitter that accumulates in the long optical paths between the bunch measurement and experiment endstation. More recently, arrival-time measurements based on transient X-ray fluence-dependent effects have been made directly on the FEL photon pulse[19–24]. However, because the FEL intensity and pulse shape change from shot to shot, these effects can be triggered at different points within the FEL emission envelope. This source of error will still be present in seeded FEL operation, where the pulse shape is expected to remain stable, but its intensity can still fluctuate significantly[25]. As a result, a timestamp of the FEL pulse arrival, regardless of accuracy, may not provide enough information to achieve sub-X-ray pulse duration time resolution in pump–probe

[1]Max-Planck Research Department for Structural Dynamics, University of Hamburg, Center for Free Electron Laser Science, Notkestrasse 85, 22607 Hamburg, Germany, [2]Max-Planck Institute of Quantum Optics, Hans-Kopfermann-Strasse 1, 85748 Garching, Germany, [3]Ludwig-Maximilians Universität München, Am Coulombwall 1, 85746 Garching, Germany, [4]Deutsches Elektronen-Synchrotron DESY, Notkestrasse 85, 22607 Hamburg, Germany, [5]European XFEL, Albert-Einstein-Ring 19, 22761 Hamburg, Germany, [6]School of Physical Science and National Center for Plasma Science and Technology (NCPST), Dublin City University, Glasnevin, Dublin 9, Ireland, [7]Departamento de Fisica de Materiales, University of the Basque Country UPV/EHU, E-20018 San Sebastian/Donostia, Spain, [8]IKERBASQUE, Basque Foundation for Science, E-48011, Bilbao, Spain, [9]Donostia International Physics Center (DIPC), E-20018 San Sebastian/Donostia, Spain, [10]Skobeltsyn Institute of Nuclear Physics, Lomonosov Moscow State University, Moscow 119991, Russia, [11]SLAC National Accelerator Laboratory, 2575 Sand Hill Road, Menlo Park, California 94025, USA; [†]These authors contributed equally to this work. *e-mail: adrian.cavalieri@mpsd.cfel.de
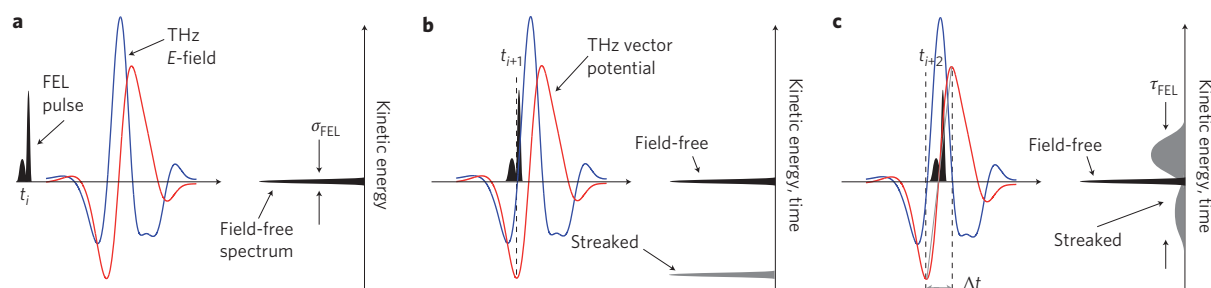
Figure 1 | Schematic of single-shot, single-cycle terahertz streaking measurement. a–c, Blue and red curves represent the electric field and corresponding vector potential of a single-cycle terahertz pulse. The vertical axis corresponds to the kinetic energy of the photoelectron emission, which is equivalent to time in streaking measurements, as depicted in **b** and **c**. In the single-shot measurement in **a**, the FEL pulse does not overlap in time with the terahertz pulse and the kinetic energy distribution of photoelectrons ejected by the FEL pulse is unaffected. In this case the measured photoelectron spectrum reveals the intrinsic bandwidth σ_{FEL} of the FEL pulse. In the single-shot measurements depicted in **b** and **c**, the FEL-induced photoemission overlaps with the streaking terahertz field and the photoelectron spectra are broadened and shifted—'streaked'—depending on their instant of release. In **b**, the FEL pulse overlaps with an extreme of the terahertz vector potential, leading to a maximally downshifted photoelectron spectrum with minimized spectral broadening. As a result, the temporal structure of the pulse is not observed in the measured spectrum. In **c**, the temporal overlap occurs near the zero crossing of the terahertz vector potential where the time of arrival as well as the temporal profile and duration, τ_{FEL}, can be accessed with the highest resolution. The temporal dynamic range of the measurement is given by the length of the terahertz vector potential half-cycle (Δt).

experiments. To ensure that the highest time resolution can be reached at FELs, it is essential to achieve full shot-to-shot temporal characterization of the X-ray pulse profile on a time base synchronized to the pump laser that drives the experiment dynamics.

We have now achieved this full temporal characterization using independent optical laser-driven single-cycle terahertz pulses for femtosecond time-resolved photoelectron spectroscopy. This unique method is implemented in a transparent inline geometry, can accommodate fluctuating X-ray pulse intensity, is applicable over the full range of photon energies produced by FELs (from the XUV to hard X-ray regime), and can be applied to pulses ranging from less than 10 fs to ~100 fs.

Ultrashort XUV pulse characterization

The measurement is adapted from attosecond metrology, where fully coherent XUV pulses generated through high-harmonic generation[26] have been characterized with attosecond precision[27,28]. In these measurements, a few-cycle laser pulse at a central wavelength of 750 nm is used to broaden and shift the initial kinetic energy distribution of photoelectrons ejected from a noble gas target by the XUV pulse. When the photoemission process that replicates the temporal structure of the ionizing XUV pulse[29] is confined to within one half-cycle of the laser field (1.25 fs for 750 nm carrier wavelength), the detected photoelectron spectrum is said to be streaked. In the classical model[30], the shift in kinetic energy of the streaked photoemission peak is governed by the amplitude of the vector potential of the streaking pulse at the instant of ionization. The degree of spectral broadening depends on both the temporal extent of the ionizing pulse and the variation of the streaking field over its duration.

Retrieval of the ionizing XUV pulse profile from the streaked spectrum requires characterization of the streaking field. For perfectly synchronized identical pulses from the same source, the streaking field is accessed through a set of sequential measurements over the full range of delays between optical and XUV pulse. As all parameters remain constant throughout the multi-shot acquisition[31], a spectrogram constructed from the series of measurements reveals the precise streaking field parameters, and the XUV pulse characteristics can subsequently be obtained for streaked spectra averaged at fixed delays with demonstrated sub-100 attosecond resolution[28,32].

Although attosecond XUV pulses produced by high-harmonic generation are confined to the half-cycle of an optical laser field, SASE FEL pulses are expected to be as long as ~100 fs. Therefore,

longer streaking fields in the terahertz regime must be used for the application of streaking techniques. Direct extension of attosecond streaking to the femtosecond regime has been achieved at FLASH by using the FEL-driving electron bunch in an additional dedicated undulator structure to generate multi-cycle, phase-stable terahertz fields for streaking[33]. The terahertz pulse is intrinsically synchronized to the electron bunch, which allows the streaking field parameters to be accessed by traditional attosecond methods. However, this synchronization does not permit access to any timing information relative to an external pump laser system. Furthermore, as the electron bunch generates the streaking field, the terahertz characteristics change as the electron beam is tuned, limiting the utility of this technique to FEL studies where beam parameters are varied systematically. In the worst case, when the accelerator is tuned for the shortest FEL pulses using very low charge and highly compressed bunches, the beam-based terahertz generation will not be strong enough for streaking. Application of this technique is complicated further, as the FEL pulse, and subsequently the terahertz streaking pulse, are generated sequentially and the FEL pulse must be delayed with respect to the terahertz pulse to allow for temporal overlap. While this is accomplished at FLASH using normal-incidence multilayer optics, these optics cannot be produced at arbitrary wavelengths or with arbitrary bandwidths, and currently cannot be produced for photon energies above ~400 eV (ref. 34).

Optical laser-driven terahertz streaking spectroscopy

FEL pulse characterization by an independent laser-driven terahertz source overcomes the limitations of streaking with accelerator-based terahertz sources, while maintaining the capability to sample 100 fs pulses. Furthermore, as laser-driven terahertz fields are locked to the external laser, the resulting FEL pulse profile measurements are given on a time base that is synchronized to the pump–probe experiment environment. To accommodate the full range of photon energies, appropriate target atoms can be chosen according to the kinetic energy spectrum of their emitted Auger electrons or photoelectrons, allowing extension of terahertz streaking into the hard X-ray regime.

In contrast to standard attosecond streaking spectroscopy, in the measurements presented here, retrieval of the calibrated FEL temporal profile is achieved without intrinsic synchronization between the ionizing pulse and the streaking field. This is enabled by using single-cycle terahertz pulses that are characterized independently by electro-optic sampling (EOS). Single-cycle terahertz pulses generated by optical rectification of femtosecond Ti:sapphire laser
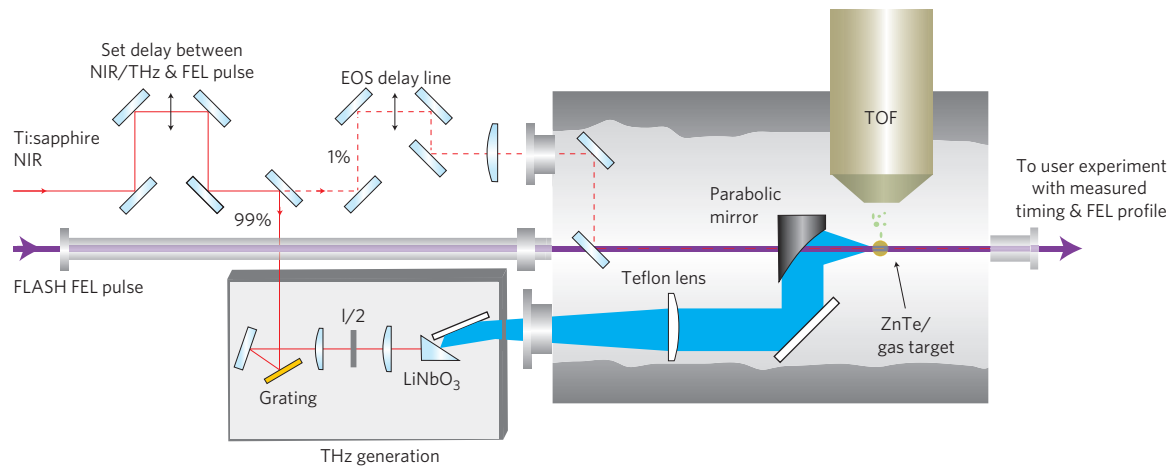
Figure 2 | Terahertz streaking experiment set-up. A Ti:sapphire NIR laser pulse, appropriately delayed with respect to the FEL pulse, is split into two parts. Most of the pulse energy is used for tilted-wavefront terahertz generation in LiNbO$_3$; the remaining part can be used for EOS of the terahertz pulse in zinc telluride (ZnTe) for *in situ* characterization. In the streaking measurement, the collinear FEL photon pulse ejects a burst of photoelectrons from the gas, with a temporal profile identical to the incident soft X-ray FEL pulse. The terahertz pulse is used to streak the photoelectron burst and consequently characterize the FEL pulse.

pulses have a streaking field half-cycle or ramp of ∼600 fs (ref. 35 and Supplementary Information), significantly longer than the maximum expected FEL pulse duration and timing jitter. As a result, once the streaking pulse and FEL pulse have been overlapped temporally, all single-shot acquisitions occur on a uniquely defined, nearly linear portion of the streaking ramp.

As illustrated in Fig. 1, overlap with the terahertz streaking ramp leads to spectral broadening, as photoelectrons ejected by the FEL pulse are subject to different streaking strengths depending on their instant of emission. Broader streaked spectra are observed by increasing the variation in streaking field strength over the FEL pulse envelope, either by increasing the temporal extent of the photoelectron emission, that is, introducing longer X-ray pulses, or by using stronger terahertz fields with steeper gradients. To take advantage of this mutual dependence and retrieve a calibrated FEL temporal profile, a streaking map is created from the terahertz electric field, measured independently by EOS, and the classical equation that governs streaking[30]:

$$E_{kin}^{shift}(t_0) = -p_i A(t_0) - \frac{A^2(t_0)}{2}, \quad \text{where} \quad A(t_0) = -\int_{t_0}^{\infty} E(t)\mathrm{d}t. \quad (1)$$

Here E_{kin}^{shift} refers to the kinetic energy shift of the photoelectron, p_i is the initial undressed momentum, $A(t_0)$ is the terahertz vector potential and E the terahertz electric field. Using this relationship, a unique transformation between the streaked kinetic energy spectrum and pump–probe experiment time base is established. When the streaked photoelectron spectra are significantly broader than the initial spectral bandwidth of the FEL photon pulse, the temporal profile of the FEL pulse can be recovered directly.

The layout of the terahertz streaking experiment at FLASH is shown in Fig. 2. An ∼3 mJ, ∼50 fs Ti:sapphire near-infrared (NIR) laser pulse is split into two parts, with 99% of the pulse used for terahertz generation and the remainder used for *in situ* EOS characterization of the terahertz pulse. To phase-match the optical rectification process, the pulse front of the driving NIR pulse is tilted with a diffraction grating and then imaged onto the LiNbO$_3$ crystal[36]. The resultant single-cycle terahertz pulse is ∼2 ps in duration, with a frequency spectrum centred at ∼0.6 THz and energy of ∼4 µJ (see Supplementary Figs S3 and S4 for details).

Undressed 2p and 2s photoemission peaks from neon were used to calibrate the time-of-flight (TOF) photoelectron spectrometer, as they

lie in the spectral region of interest. However, helium was used for the streaking measurement because it has an isolated photoemission line, which avoids the possibility of photoelectrons from different binding energies overlapping with each other when they are broadened during streaking. Approximately 10 µJ soft X-ray FEL pulses[37] at 4.8 nm (258 eV) with an independently measured average bandwidth of ∼2.5 eV full-width at half-maximum (FWHM; ref. 38) were used to eject the He 1s electrons with an initial kinetic energy of ∼233 eV. The terahertz and FEL pulses were polarized along the direction of detection such that the streaking effect coupled directly to the observed photoelectron kinetic energy.

For short periods of time, during which thermal and other environmental drifts are negligible, the optical laser and terahertz streaking pulse that it produces (as well as the FEL pulse) are electronically synchronized to a common radiofrequency distribution network[39,40] at the accelerator facility to within ∼100 fs r.m.s. By taking advantage of this coarse electronic synchronization, spectra were recorded as the desired delay between terahertz and soft X-ray pulses was varied in 100 fs steps. Approximately 400
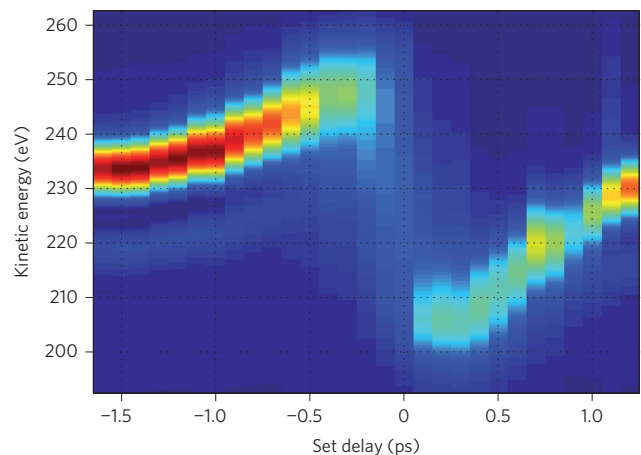

Figure 3 | Averaged spectrogram. Streaked photoelectron spectra of He as a function of set delay between the terahertz streaking pulse and ionizing FEL pulse at FLASH. Coarse synchronization between the FEL pulse and streaking pulse was maintained electronically during the scan to ∼100 fs r.m.s. Each time slice is an average of ∼400 single-shot measurements.

single-shot spectra were collected at each delay step and combined to generate the averaged spectrogram shown in Fig. 3. For large delays, where the terahertz field is weak, the He 1s photoemission peak is nearly unaffected and located near its undressed, field-free kinetic energy. Around the zero crossing of the vector potential, the kinetic energy of the photoelectrons is shifted and broadened depending on the terahertz streaking field parameters.

The streaking map was constructed using equation (1) and the terahertz electric field measured by EOS. Although the shape of the measured electric field is exact, measurement of the absolute peak electric field strength is less precise due to imperfect orientation and impurities in the electro-optic crystal that result in a reduced effective electro-optic coefficient. Therefore, the single-shot photoelectron spectra from the full time scan that experience the greatest positive or negative kinetic energy shift are used to scale the amplitude of the streaking map. This additional measurement allows us to determine the absolute electric field strength with much greater accuracy than by EOS alone. The streaking map used in our measurements spans the maximum observed single-shot shift of the photoemission peak of $+23/-37$ eV, corresponding to a peak terahertz electric field strength of 165 kV cm^{-1}.

The resolution of the timing measurements is limited by both the strength of the terahertz streaking field, or degree of spectral broadening, and the energy resolution of the photoelectron spectrometer. In these experiments, the energy resolution of the photoelectron spectrometer can be determined by comparing the bandwidth of the average field-free photoelectron spectrum of the He 1s line to an independent measurement of the average FEL photon bandwidth. The unstreaked, field-free photoelectron spectrum is nearly Gaussian with an observed bandwidth of 7.2 eV FWHM, which is a convolution of the energy resolution with the FEL bandwidth. Because the independently measured FEL bandwidth is 2.5 eV FWHM, the photoelectron spectrometer resolution is 6.8 eV FWHM. The energy resolution of the photoelectron spectrometer in conjunction with the terahertz streaking map is used to determine the minimum separation between two distinguishable features in the FEL pulse temporal profile. In these measurements, the minimum separation is ∼40 fs. It is expected that this resolution limit can be improved to better than 10 fs.

Complete single-shot FEL temporal pulse characterization

Characteristic streaking measurements made at FLASH are shown in Fig. 4. Figure 4a,c shows the streaked single-shot spectra of two different FEL pulses. The statistical error in the single-shot spectrum is calculated according to the number of electrons collected within the energy resolution window of the detector. Because the photoelectron spectrum is heavily oversampled, boxcar integration is
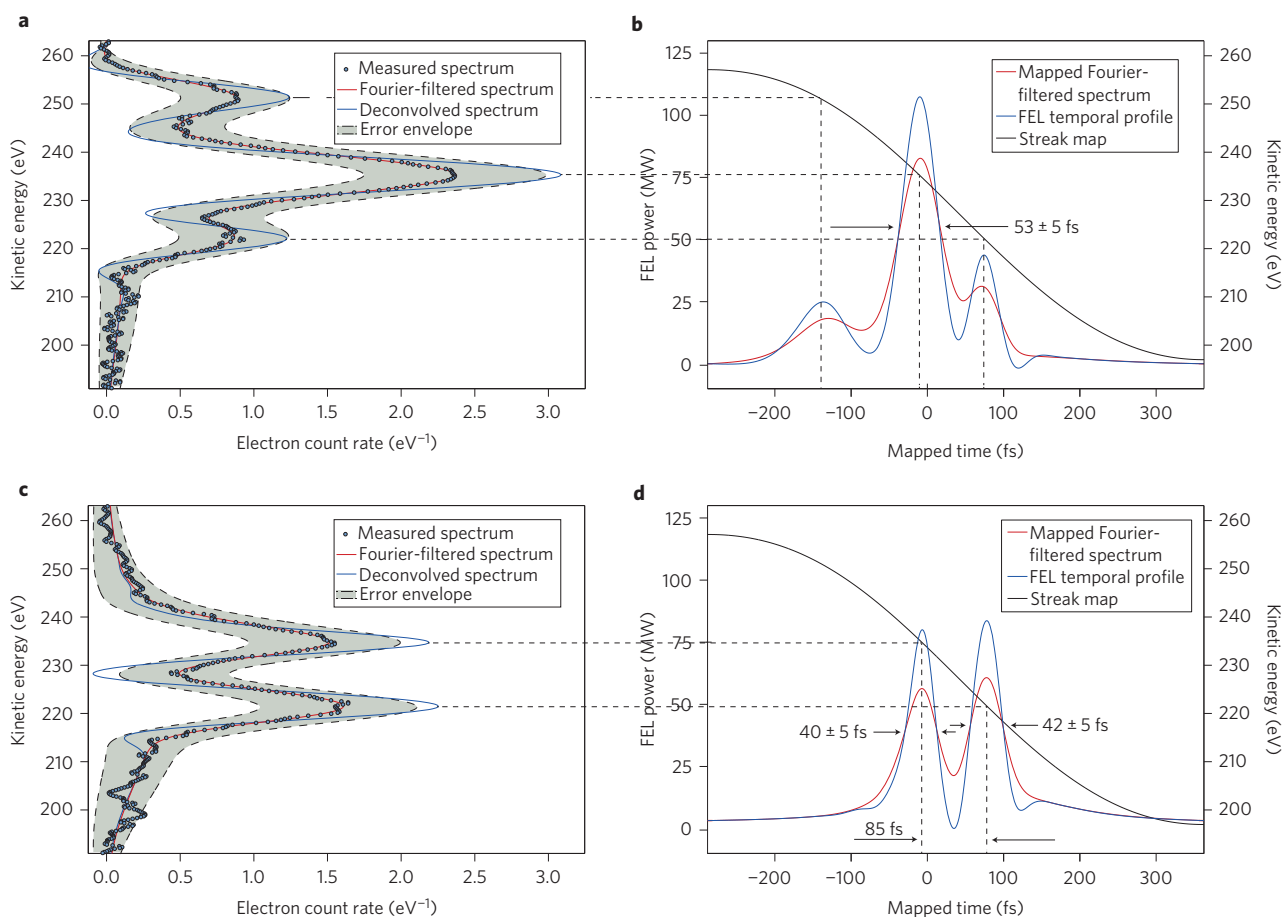

Figure 4 | Single-shot FEL pulse power profile on the pump–probe laser time base. a,c, Two distinct single-shot streaked photoelectron spectra. Shaded error envelopes are calculated by boxcar integration based on the number of electrons collected within the 6.8 eV FWHM resolution window of the time-of-flight spectrometer. Blue dots are raw data points in the measured streaked spectra. Red curves show the spectra after Fourier filtering to remove high-frequency noise. Blue curves are filtered streaked spectra following deconvolution of the photoelectron spectrometer resolution. **b,d,** Retrieved FEL pulse profiles on the pump–probe laser time base using the single-valued streaking map (black dashed curve). Scales on the right correspond to the streaking map; scales on the left correspond to the FEL power that is obtained by assuming 10 μJ of pulse energy for the single-shot measurement shown in **a**. A 53±5 fs FWHM substructure is observed in the first single-shot measurement and a ∼40±5 fs FWHM substructure in the second.
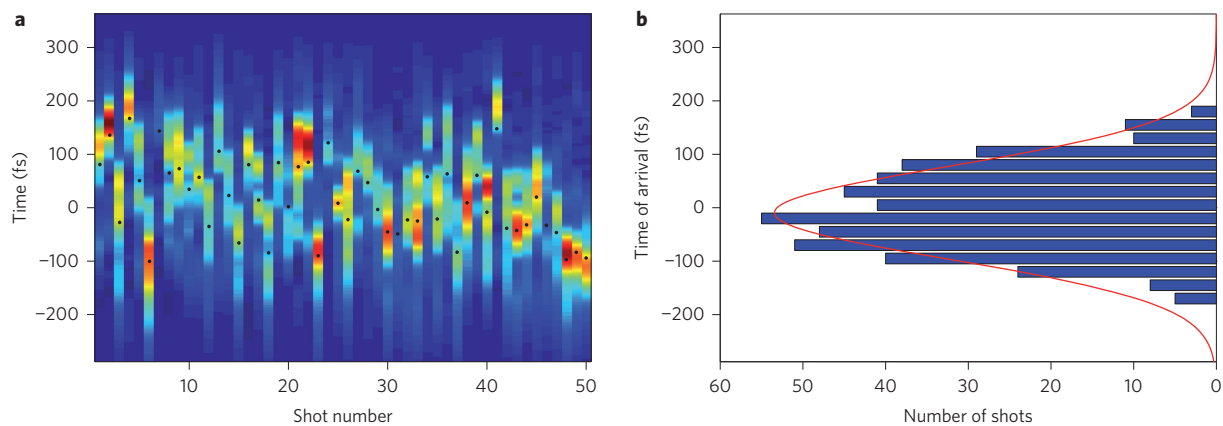
Figure 5 | Measured arrival time jitter. a, False-colour plot of 50 consecutive single-shot measurements made near time zero. The centre of mass of the individual profiles (black points) is used to evaluate the arrival time of each pulse. **b**, Distribution of arrival times collected over ∼450 consecutive shots. The Gaussian fit to the distribution (red curve) has a corresponding width of ∼87 fs r.m.s., which is a measure of the short-term timing jitter between the pump–probe laser and the FEL.

performed across the spectrum, resulting in a smooth error envelope that bounds the measured spectrum.

To recover the FEL pulse profile, the energy resolution of the TOF spectrometer is first deconvolved from the measured streaked photoelectron spectra as shown in Fig. 4. Figure 4b,d show the corresponding transformation of the measured and deconvolved spectra to time. In the temporal profile plots, positive time corresponds to the leading edge of the soft X-ray pulse. The FEL pulse in Fig. 4b exhibits a dominant central feature at 53 ± 5 fs FWHM, with weaker satellite features at ∼100 fs from the main peak. In contrast, the other displayed FEL pulse exhibits nearly equal peaks with individual durations of ∼40 ± 5 fs FWHM separated by ∼85 fs in time. The accuracy of these measurements is determined from the upper and lower statistical error bounds on the streaked photoelectron spectrum (for details see Methods).

The structure observed in these FEL pulses is not caused by individual longitudinal FEL emission modes, which would typically have a duration of ∼5 fs for the operating parameters at FLASH. Rather, the structure is due to uneven soft X-ray amplification over the length of the electron bunch caused by small variations in its composition and inherent instability in the highly nonlinear SASE process. During these particular measurements, the FEL was operating in the exponential gain regime, where it is particularly sensitive to electron beam parameters[41,42]. This mode of operation serves as an ideal test of the utility of these streaking measurements, as the pulse-to-pulse FEL fluctuations are more severe and the FEL flux is relatively low. Under normal saturated user operation with higher flux, the measurement is expected to be even more reliable, as the number of detected photoelectrons will increase.

The accuracy of the pulse arrival information is governed by the stability of the terahertz streaking field and fluctuation in the mean FEL photon energy, which results in a photoelectron kinetic energy offset and corresponding temporal offset. The stability of the terahertz pulse is a function of the driving optical laser. In these experiments, the optical laser pulse energy was measured to be stable to within 1% r.m.s. For saturated terahertz generation, as was the case in these measurements, the terahertz field scales with the square root of the driving laser pulse energy. As a result, the terahertz field is stable to within 0.5% r.m.s. and its fluctuation can be neglected when considering the stability of the transformed time base. However, the FEL photon energy during these measurements fluctuated from shot to shot at a level of 1 eV r.m.s. (ref. 38); this constitutes the main source of uncertainty in the time base of the retrieved FEL pulse profile of ∼6 fs r.m.s. Using existing technology, this uncertainty can be significantly reduced with online

measurement of the single-shot FEL photon spectrum. It should also be noted that fluctuation in the FEL photon energy has a minimal effect on the retrieved pulse profile, as the streaking map transformation is nearly linear at the zero crossing, and a small offset in the kinetic energy does not affect the spectral broadening due to streaking.

These streaking measurements can be used at FLASH to assess the timing jitter between the external pump–probe laser and the FEL pulse. For this particular purpose, we ignore fluctuations in the pulse shape, and the arrival of the FEL pulse is clocked by calculating the centre-of-mass of the retrieved FEL pulse temporal profile. The arrival times of ∼450 consecutive FEL pulses measured near time zero in the delay scan shown in Fig. 3 are calculated and displayed in Fig. 5. The distribution of arrival times has a width of 87 fs r.m.s., which is consistent with the expected performance of the electronic laser synchronization[17].

Discussion and outlook

In the future, laser-based terahertz streaking measurements may be improved to allow the characterization of a fundamental FEL pulse substructure separated by only several femtoseconds, by increasing the energy resolution of the photoelectron spectrometer and also by increasing the terahertz streaking strength. A number of advances in terahertz generation[43] and photoelectron spectroscopy currently indicate that significant improvements in our measurement technique could be realized in the near future. Single-shot photoelectron detection at FELs has recently been demonstrated at an energy resolution of $\Delta E/E = 0.4\%$ (ref. 44), an improvement of nearly an order of magnitude in comparison to the energy resolution achieved in these experiments. Stronger, steeper streaking fields can be achieved by decreasing the rise time of the streaking ramp[45] or by scaling up the terahertz field strength with stronger driving optical laser pulses. Using the tilted pulse-front method and advanced focusing, fields exceeding 1 MV cm^{-1} have been achieved[46].

Optical laser-driven terahertz streaking is currently the only method that can provide full temporal characterization of FEL photon pulses, which is crucial for their most effective and complete utilization. This technique is implemented with standard laser technology and the apparatus does not require dedicated accelerator infrastructure. Furthermore, this method is ideally suited for use as a diagnostic for machine studies and FEL optimization for specific lasing parameters and pulse shapes, as it is completely decoupled from all other FEL parameters. Because the measurement is made in transmission geometry and does not affect the FEL pulse,

it can be used as a standard diagnostic between the FEL source and user experiments. As a result, it will be possible to perform experiments with sub-pulse duration time resolution, and also to post-process arbitrary experimental data based on the true single-shot FEL intensity profile.

Methods

Error analysis. The statistical error in the single-shot photoelectron spectra was evaluated by counting the number of detected photoelectrons within the 6.8 eV energy resolution window of the detector by boxcar integration centred at each collected data point. As the spectra were heavily oversampled (275 data points were collected within the ~60 eV streaked kinetic energy range), an error envelope was generated rather than discrete points with individual error bars.

The 6.8 eV photoelectron spectrometer energy resolution was deconvolved from the upper and lower bound of the error envelope in addition to the measured spectrum and mapped to time. Mapping the error envelope provides an upper and lower bound of the pulse temporal profile. Following this procedure, the width of the central peak in the measurement shown in the main text (Fig. 4b)—53 fs FWHM— was found to have upper and lower bounds of 58 and 48 fs FWHM, respectively. Based on this analysis, we conclude that the temporal profile was measured with an accuracy of ± 5 fs FWHM. This procedure is illustrated in Supplementary Fig. S2.

References

1. Ackermann, W. *et al.* Operation of a free-electron laser from the extreme ultraviolet to the water window. *Nature Photon.* **1,** 336–342 (2007).
2. Emma, P. *et al.* First lasing and operation of an angstrom-wavelength free-electron laser. *Nature Photon.* **4,** 641–647 (2010).
3. Pile, D. X-rays first light from SACLA. *Nature Photon.* **5,** 456–457 (2011).
4. Ishikawa, T. *et al.* A compact X-ray free-electron laser emitting in the sub-ångström region. *Nature Photon.* **6,** 540–544 (2012).
5. Ding, Y. *et al.* Measurements and simulations of ultralow emittance and ultrashort electron beams in the Linac Coherent Light Source. *Phys. Rev. Lett.* **102,** 254801 (2009).
6. Emma, P. *et al.* Femtosecond to subfemtosecond X-ray pulses from a self-amplified spontaneous-emission-based free-electron laser. *Phys. Rev. Lett.* **92,** 074801 (2004).
7. Meyer, M. *et al.* Angle-resolved electron spectroscopy of laser-assisted Auger decay induced by a few-femtosecond X-ray pulse. *Phys. Rev. Lett.* **108,** 063007 (2012).
8. Först, M. *et al.* Driving magnetic order in a manganite by ultrafast lattice excitation. *Phys. Rev. B* **84,** 241104 (2011).
9. Rohringer, N. *et al.* Atomic inner-shell X-ray laser at 1.46 nanometres pumped by an X-ray free-electron laser. *Nature* **481,** 488–491 (2012).
10. Vinko, S. M. *et al.* Creation and diagnosis of a solid-density plasma with an X-ray free-electron laser. *Nature* **482,** 59–U75 (2012).
11. Young, L. *et al.* Femtosecond electronic response of atoms to ultra-intense X-rays. *Nature* **466,** 56–U66 (2010).
12. Neutze, R., Wouts, R., van der Spoel, D., Weckert, E. & Hajdu, J. Potential for biomolecular imaging with femtosecond X-ray pulses. *Nature* **406,** 752–757 (2000).
13. Siebert, M. M. *et al.* Single mimivirus particles intercepted and imaged with an X-ray laser. *Nature* **470,** 78–U86 (2011).
14. Barty, A. *et al.* Self-terminating diffraction gates femtosecond X-ray nanocrystallography measurements. *Nature Photon.* **6,** 35–40 (2012).
15. Saldin, E. L., Schneidmiller, E. A. & Yurkov, M. V. Statistical and coherence properties of radiation from x-ray free-electron laser. *New J. Phys.* **12,** 035010 (2010).
16. Cavalieri, A. L. *et al.* Clocking femtosecond X-rays. *Phys. Rev. Lett.* **94,** 114801 (2005).
17. Azima, A. *et al.* Time resolved pump–probe experiments beyond the jitter limitations at FLASH. *Appl. Phys. Lett.* **94,** 144102 (2009).
18. Tavella, F., Stojanovic, N., Geloni, G. & Gensch, M. Few femtosecond timing at fourth-generation X-ray light sources. *Nature Photon.* **5,** 162–165 (2011).
19. Radcliffe, P. *et al.* Single-shot characterization of independent femtosecond extreme ultraviolet free electron and infrared laser pulses. *Appl. Phys. Lett.* **90,** 131108 (2007).
20. Gahl, C. *et al.* A femtosecond X-ray/optical cross-correlator. *Nature Photon.* **2,** 165–169 (2008).
21. Maltezopoulos, T. *et al.* Single-shot timing measurement of extreme-ultraviolet free-electron laser pulses. *New J. Phys.* **10,** 033026 (2008).
22. Bionta, M. R. *et al.* Spectral encoding of X-ray/optical relative delay. *Opt. Express* **19,** 21855–21865 (2011).
23. Schorb, S. *et al.* X-ray-optical cross-correlator for gas-phase experiments at the Linac Coherent Light Source free-electron laser. *Appl. Phys. Lett.* **100,** 121107 (2012).
24. Beye, M. *et al.* X-ray pulse preserving single-shot optical cross-correlation method for improved experimental temporal resolution. *Appl. Phys. Lett.* **100,** 121108 (2012).
25. Amann, J. *et al.* Demonstration of self-seeding in a hard-X-ray free-electron laser. *Nature Photon.* **6,** 693–698 (2012).
26. Christov, I., Murnane, M. M. & Kapteyn, H. C. High-harmonic generation of attosecond pulses in the 'single-cycle' regime. *Phys. Rev. Lett.* **78,** 1251–1254 (1997).
27. Kienberger, R. *et al.* Atomic transient recorder. *Nature* **427,** 817–821 (2004).
28. Goulielmakis, E. *et al.* Single-cycle nonlinear optics. *Science* **320,** 1614–1617 (2008).
29. Schultze, M. *et al.* Delay in photoemission. *Science* **328,** 1658–1662 (2010).
30. Itatani, J. *et al.* Attosecond streak camera. *Phys. Rev. Lett.* **88,** 173903 (2002).
31. Baltuska, A. *et al.* Attosecond control of electronic processes by intense light fields. *Nature* **421,** 611–615 (2003).
32. Gagnon, J., Goulielmakis, E. & Yakovlev, V. S. The accurate FROG characterization of attosecond pulses from streaking measurements. *Appl. Phys. B* **92,** 25–32 (2008).
33. Frühling, U. *et al.* Single-shot terahertz-field-driven X-ray streak camera. *Nature Photon.* **3,** 523–528 (2009).
34. Eriksson, F. *et al.* Atomic scale interface engineering by modulated ion-assisted deposition applied to soft X-ray multilayer optics. *Appl. Opt.* **47,** 4197–4204 (2008).
35. Planken, P., Nienhuys, H., Bakker, H. & Wenckebach, T. Measurement and calculation of the orientation dependence of terahertz pulse detection in ZnTe. *J. Opt. Soc. Am. B* **18,** 313–317 (2001).
36. Yeh, K. L., Hoffmann, M. C., Hebling, J. & Nelson, K. A. Generation of 10 μJ ultrashort terahertz pulses by optical rectification. *Appl. Phys. Lett.* **90,** 171121 (2007).
37. Tiedtke, K. *et al.* Gas-detectors for X-ray lasers. *J. Appl. Phys.* **103,** 094511 (2008).
38. Nicolosi, P. *et al.* Grazing-incidence spectrometer for the monitoring of the VUV FEL beam at DESY. *J. Electron Spectrosc. Rel. Phenom.* **144,** 1055–1058 (2005).
39. Spence, D. E., Sleat, W. E., Evans, J. M., Sibbett, W. & Kafka J. D. Time synchronization measurements btween 2 self-modelocked Ti:sapphire lasers. *Opt. Commun.* **101,** 286–296 (1993).
40. Ma, L-S. *et al.* Sub-10 femtosecond active synchronization of two passively mode-locked Ti:sapphire oscillators. *Phys. Rev. A* **64,** 021802(R) (2001).
41. Bonifacio, R., Pellegrini C. & Narducci, L. Collective instabilities and high-gain regime in a free electron laser. *Opt. Commun.* **50,** 373–378 (1984).
42. Kim, K-J. An analysis of self-amplified spontaneous emission. *Nucl. Instrum. Methods A* **250,** 396–403 (1986).
43. Hoffmann, M. C. & Fulop, J. A. Intense ultrashort terahertz pulses: generation and applications. *J. Phys. D* **44,** 083001 (2011).
44. Duesterer, S. *et al.* Femtosecond X-ray pulse length characterization at the Linac Coherent Light Source free-electron laser. *New J. Phys.* **13,** 093024 (2011).
45. Hauri, C. P., Ruchert, C., Vicario, C. & Ardana, F. Strong-field single-cycle THz pulses generated in an organic crystal. *Appl. Phys. Lett.* **99,** 161116 (2011).
46. Hirori, H., Doi, A., Blanchard, F. & Tanaka, K. Single-cycle terahertz pulses with amplitudes exceeding 1 MV/cm generated by optical rectification in LiNbO(3). *Appl. Phys. Lett.* **99,** 091106 (2011).

Author contributions

A.L.C., M.C.H. and H.S. conceived the project. I.G. and M.C.H. designed and executed the experiments. C.B., A.L.C., J.T.C, S.D., T.J.K., A.R.M., M.M., T.M., P.R., H.S. and Th.T. assisted in experimental realization. C.B., A.L.C., I.G., M.C.H., A.K.K., N.M.K., A.R.M., T.M., M.M., H.S. and Th.T. analysed and/or interpreted the data. A.L.C., S.D. and M.M. contributed materials to the experiments. A.L.C., J.T.C., I.G., M.C.H., M.M., H.S. and Th.T. wrote the paper.

Additional information

Supplementary information is available in the online version of the paper. Reprints and permission information is available online at http://www.nature.com/reprints. Correspondence and requests for materials should be addressed to A.L.C.

Competing financial interests

The authors declare no competing financial interests.